

Pt(II), Pd(II) and UO₂(II) complexes of N,N'-bis(2-pyridyl)thiourea; structural, thermal and biological studies

Usama El-Ayaan*

Department of Chemistry, Faculty of Science, Mansoura University, Mansoura 35516, Egypt

Department of Chemistry, College of Science, King Faisal University, P.O. Box 380, Hofuf 31982, Saudi Arabia

ARTICLE INFO

Article history:

Received 3 March 2011

Received in revised form 29 March 2011

Accepted 16 April 2011

Available online 22 April 2011

Keywords:

Thiourea complexes

Spectroscopy

Thermal analysis

Antibacterial

ABSTRACT

Novel complexes of Pt²⁺, Pd²⁺ and UO₂²⁺ with N,N'-bis(2-pyridyl)thiourea (H₂BPT) **1** were synthesized. These complexes namely [Pt(HBPT)₂] **2**, [Pd(HBPT)₂] **3** and [UO₂(HBPT)(OAc)(H₂O)] **4**, were characterized by elemental analysis and spectral measurements. Suggested structures (square-planar for both **2** and **3** complexes and pentagonal-bipyramidal geometry for **4**) were confirmed by applying geometry optimization and conformational analysis.

Thermal properties and decomposition kinetics of all compounds are investigated. The interpretation, mathematical analysis and evaluation of kinetic parameters (*E*, *A*, ΔH , ΔS and ΔG) of all thermal decomposition stages have been evaluated using Coats–Redfern, Horowitz–Metzger and MKN methods. The biochemical studies showed that, complex **2** has powerful and complete degradation effect on DNA. The antibacterial screening demonstrated that, complex **2** has the maximum and broad range activities against Gram-positive and Gram-negative bacterial strains.

© 2011 Elsevier B.V. All rights reserved.

1. Introduction

Thioureas are recognized for their inter- and intra-molecular hydrogen-bonding. In addition, they can act as ligands in coordination complexes. This combination has led to their increasing use in an array as self-assembled network materials [1]. Thiourea complexes with transition metal atoms are also subject of interest because of the special roles played by these kinds of compounds in biological processes [2–4]. Recently, extensive studies [5–7] on the structures of N,N'-bis(substituted 2-pyridyl)thioureas and their intra-molecular and inter-molecular hydrogen bonding interactions have been published. The ligational behavior and the X-ray single crystal structures of copper(I) and zinc(II) complexes with N,N'-bis(2-pyridyl) thiourea, have been reported [8].

In this paper we prepared new complexes of Pt²⁺, Pd²⁺ and UO₂²⁺ with N,N'-bis(2-pyridyl) thiourea (H₂BPT) (Fig. 1). Very pure solid complexes were obtained but unfortunately crystals suitable for X-ray measurements were not available. We apply geometry optimization and conformational analysis to the free ligand and all studied complexes as a further tool to confirm the proposed structures.

The interpretation, mathematical analysis and evaluation of kinetic parameters (*E*, *A*, ΔH , ΔS and ΔG) of all thermal decomposition stages have been evaluated using Coats–Redfern, Horowitz–Metzger and MKN methods.

2. Theoretical

2.1. Thermal degradation kinetics

Non-isothermal methods have been extensively used for the evaluation of kinetic parameters of decomposition reactions. The rate of degradation or conversion, dx/dt , is a linear function of temperature-dependant rate constant *k*, and a temperature-independent function of conversion α , and can be described as follow [9]:

$$\frac{dx}{dt} = k(T)f(\alpha) \quad (1)$$

The reaction rate constant, *k*, has been described by the Arrhenius expression

$$k = A e^{-E/RT} \quad (2)$$

where *R* is the gas constant in (J mol⁻¹ K⁻¹). Substituting Eq. (2) into Eq. (1), we get

$$d\alpha/dt = A(e^{-E/RT})f(\alpha) \quad (3)$$

* Present address: Department of Chemistry, College of Science, King Faisal University, P.O. Box 380, Hofuf 31982, Saudi Arabia. Tel.: +996 553901011; fax: +966 35886437.

E-mail address: uelayaan@kfu.edu.sa

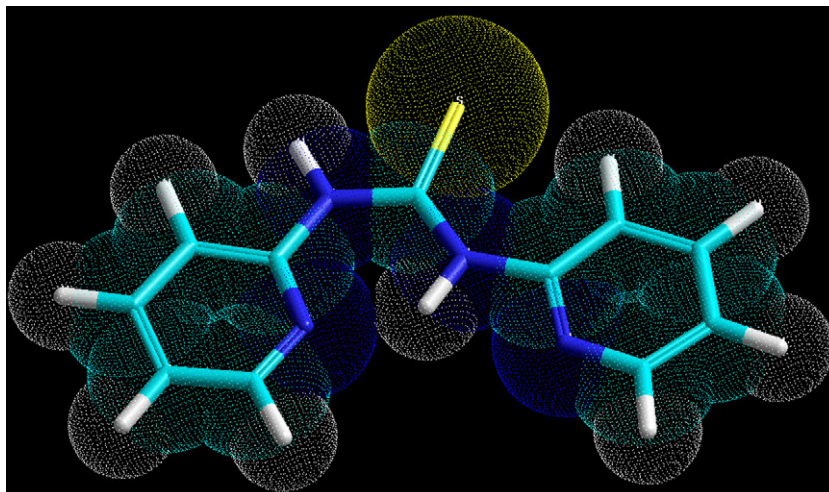


Fig. 1. Structure of the free ligand (H₂BPT).

If the temperature of the sample is changed by a controlled and constant heating rate, $\varphi = dT/dt$, the variation of the degree of conversion can be analyzed as a function of temperature, this temperature being dependant on the time of heating. Therefore, the rearrangement of Eq. (3) gives

$$d\alpha/dt = \frac{A}{\varphi} (e^{-E/RT}) f(\alpha) \quad (4)$$

The integrated form of Eq. (4) is generally expressed as

$$g(\alpha) = \int_0^\alpha \frac{d\alpha}{f(\alpha)} = \left(\frac{A}{\varphi}\right) \int_0^T e^{-E/RT} dT \quad (5)$$

where $g(\alpha)$ is the integrated form of the conversion dependence function. The integral on the right-hand side of Eq. (5) is known as temperature integral and has no closed form solution. Several techniques have been used for the evaluation of temperature integral. Most commonly used methods for this purpose are integral method of Coats–Redfern [10], the approximation method of Horowitz–Metzger [11] and MKN equation [12].

In the present investigation, kinetic parameters have been evaluated using the following three methods and the results obtained by these methods are compared with one another. The following three methods are discussed in brief.

2.1.1. Coats–Redfern equation

The Coats–Redfern equation, which is a typical integral method, can be represented as

$$\int_0^\infty d\alpha(1-\alpha)^n = (A/\varphi) \int_{T_1}^{T_2} e^{-E/RT} dt \quad (6)$$

For convenience of integration the lower term T_1 is usually taken as zero. This equation on integration gives,

$$\ln[-\ln(1-\alpha)/T^2] = -E/RT + \ln[AR/\varphi E] \quad (7)$$

A plot of left-hand side (LHS) against $1/T$ was drawn. E was calculated from the slope and A from the intercept value. The entropy of activation ΔS was calculated by using the equation:

$$\Delta S = R[\ln(Ah/kT_s)] \quad (8)$$

where k is the Boltzmann's constant and h is the Planck's constant and T_s is the DTG peak temperature [13].

2.1.2. Horowitz–Metzger equation

The Horowitz–Metzger equation is an illustrative of the approximation methods. These authors derived the relation:

$$\log\{[1 - (1-\alpha)^{1-n}]/(1-n)\} = E\theta/2.303RT_s^2 \quad \text{for } n \neq 1 \quad (9)$$

When $n = 1$, the LHS of Eq. (9) would be $\log[-\log(1-\alpha)]$. For first-order kinetics process the Horowitz–Metzger equation maybe written in the form:

$$\log[\log(w_\alpha/w_\gamma)] = E\theta/2.303RT_s^2 - \log 2.303 \quad (10)$$

where $\theta = T - T_s$, $w_\gamma = w_\alpha - w$, w_α is the mass loss at the completion of the reaction, and w is the mass loss up time t . the plot of $\log[\log(w_\alpha/w_\gamma)]$ versus θ was drawn and found to be linear from the slope of which E was calculated. The pre-exponential factor, Z , is calculated from the equation [14].

$$\frac{E}{RT_s^2} = \frac{Z}{\theta} e^{-E/RT_s} \quad (11)$$

2.1.3. MKN equation

Evaluation of the temperature integral (the right-hand side of Eq. (5)) have been evaluated using the numerical solution method. In this method, the rate equation, Eq. (4), was integrated as:

$$g(\alpha) = \frac{AE_a}{\varphi R} \left[\frac{-e}{x} + \int_\infty^x \frac{e^x}{x} dx \right] = \frac{AE_a}{\varphi R} p(x) \quad (12)$$

where $x = E_a/RT$

Madhusudanan et al. [12] have proposed a new simple approximation Eq. (13) for solving the $p(x)$ function.

$$p(x) = \frac{e^{-x}}{x^2} \left[\frac{(x+1)}{(x+3)} \right] \quad (13)$$

It has been shown that $\ln p(x)$ is a linear function of x and the slope and intercept of $\ln p(x)$ versus x curves are linear function of $1/x$ and $\ln(x)$, respectively. On combining these, the Eq. (14) was obtained

$$\ln p(x) = a + bx + c \ln x \quad (14)$$

On substituting the numerical values of a , b , and c , values of $p(x)$ were determined which was substituted in Eq. (11) and rearranged to get Madhusudanan Krishnan–Ninan (MKN) Eq. (15).

$$\ln \frac{g(x)}{T^{1.9215}} = \ln \left(\frac{AE}{\varphi R} \right) + 3.7721 - 1.9215 \ln E - 0.120394 \left(\frac{E}{T} \right) \quad (15)$$

The plot of the left-hand side of Eq. (14) against $1/T$ gives a straight line (the slope is equal to $-0.120394E$ and the intercept equals $\ln(AE/\varphi R) + 3.7721 - 1.9215 \ln E$ which on simplification gives intercept $= \ln(A/\varphi) + 0.9215 \ln E + -1.654$, E and A can be calculated from the slope and intercept, respectively.

In all complexes, the enthalpy (ΔH) and the free energy of activation (ΔG) were calculated using the following relations, respectively:

$$\Delta H = E - RT$$

$$\Delta G = \Delta H - T\Delta S$$

2.2. Molecular modeling

An attempt to gain a better insight on the molecular structure of H_2BPT ligand and its complexes, geometry optimization and conformational analysis has been performed by the use of MM+[15] force field as implemented in hyperchem 7.5 [16].

3. Experimental

3.1. Instrumentation and materials

All starting materials were purchased from Fluka, Riedel and Merck and used as received. Elemental analyses (C, H and N) were performed on a Perkin-Elmer 2400 Series II Analyzer. Infrared spectra were recorded on a Perkin-Elmer FTIR Spectrometer 2000 as KBr pellets and as Nujol mulls in the $4000\text{--}200\text{ cm}^{-1}$ spectral range. ^1H NMR measurements at room temperature were obtained on a Jeol JNM LA 300 WB spectrometer at 250 MHz, using a 5 mm probe head in CDCl_3 . Electronic spectra were recorded on a UV-UNICAM 2001 spectrophotometer using 10 mm pass length quartz cells at room temperature. Thermogravimetric (TG) and differential (DTG) thermogravimetric analysis were performed on a DTG-50 Shimadzu instrument at heating rate of $10\text{ }^\circ\text{C}/\text{min}$.

3.2. Preparation of the free ligand, N,N' -bis(2-pyridyl)thiourea (H_2BPT)

2-aminopyridine (0.2 mol, 19 g), carbon disulfide (0.1 mol, 6 mL) and triethylamine (0.1 mol, 15 mL) were refluxed for 48 h. Excess of carbon disulfide was removed by rotary evaporator (Fig. 2). It was then diluted with water 100 mL and cooled. Then the solid off-white needles of N,N' -bis(2-pyridyl) thiourea was

collected and washed with water, m.p. $158\text{ }^\circ\text{C}$, yield 18 g (78.3%), $\text{C}_{11}\text{H}_{10}\text{N}_4\text{S}$ (230.3) calcd: C 57.37, H 4.38, N 24.33, S 13.92; found C 57.60, H 4.30, N 24.50, S 13.75 – ^1H NMR (DMSO- d_6 , 500 MHz) $\Delta = 7.14$ (s, 2H, H_{py}), 7.81–7.84 (m, 3H, H_{py}), 8.34 (s, 3H, H_{py}), 11.15 (br s, 1H, NH), 14.21 (br s, 1H, SH).

3.3. Synthesis of metal complexes

Complexes were prepared by refluxing H_2BPT (0.23 g, 1.0 mmol) and 1.0 mmol of metal salt; 0.42 g of K_2PtCl_4 , 0.32 g of K_2PdCl_4 or 0.42 of $\text{UO}_2(\text{CH}_3\text{COO})_2 \cdot 2\text{H}_2\text{O}$ in 20 ml ethanol for 6 h. The resulting metal complexes were filtered off while hot, washed with ethanol followed by diethyl ether and dried in vacuo over CaCl_2 . ^1H NMR (DMSO- d_6 , 500 MHz) for complex **2** (Fig. 3); $\delta = 12.3$ (br s, 1H, NH), 12.7 (br s, 1H, NH), 7.2–8.5 (pyridyl protons, 16H), for complex **3** (Fig. 4), $\delta = 12.0$ (br s, 1H, NH), 12.6 (br s, 1H, NH), 7.1–8.4 (pyridyl protons, 16H) and for complex **4** (Fig. 5); $\delta = 10.3$ (br s, 1H, NH), 7.0–8.6 (pyridyl protons, 8H), 2.86 (s, 3H, CH_3).

3.4. Biological studies

3.4.1. DNA electrophoreses

3.4.1.1. Agarose gel. The free (H_2BPT) ligand or its Pt(II), Pd(II) and UO_2 (II) complexes ($100\text{ }\mu\text{M}$) were added individually to $1\text{ }\mu\text{g}$ of the DNA isolated from *Escherichia coli*. These samples were incubated for 1 h at $37\text{ }^\circ\text{C}$. The DNA was analyzed by using horizontal agarose gels electrophoresis. The electrophoresis was performed using 0.7% (w/v) agarose gels in TAE buffer ($5\text{ }\mu\text{M}$ sodium acetate, $1\text{ }\mu\text{M}$ EDTA and 0.04 M Tris-HCl pH 7.9). The agarose gels were stained with ethidium bromide ($0.5\text{ }\mu\text{g}/\text{mL}$) and the DNA was visualized on a UV transilluminator [17].

3.4.2. Protein gel electrophoresis

Bovine serum albumin (BSA) (3 mg) was treated with the free (H_2BPT) ligand or its Pt(II), Pd(II) and UO_2 (II) complexes ($100\text{ }\mu\text{M}$) individually. The reaction mixture was incubated for 1 h at $37\text{ }^\circ\text{C}$. The protein samples were analyzed using vertical one dimensional SDS-polyacrylamide gel electrophoresis according to the method of Laemmli [18].

The samples were prepared by adding $15\text{ }\mu\text{L}$ $2 \times$ SDS-gel loading buffer (100 mM Tris-HCl pH 6.8, 4% (w/v) SDS, 0.2% (w/v) bromophenol blue, 20% (v/v) glycerol, 200 mM DTT) and $15\text{ }\mu\text{L}$ protein samples and boiled in water bath for 3 min, $20\text{ }\mu\text{L}$ of denatured protein samples were loaded into the gel.

3.4.3. Antibacterial effect

The antibacterial investigation of the free (H_2BPT) ligand or its Pt(II), Pd(II) and UO_2 (II) complexes was carried out using cup

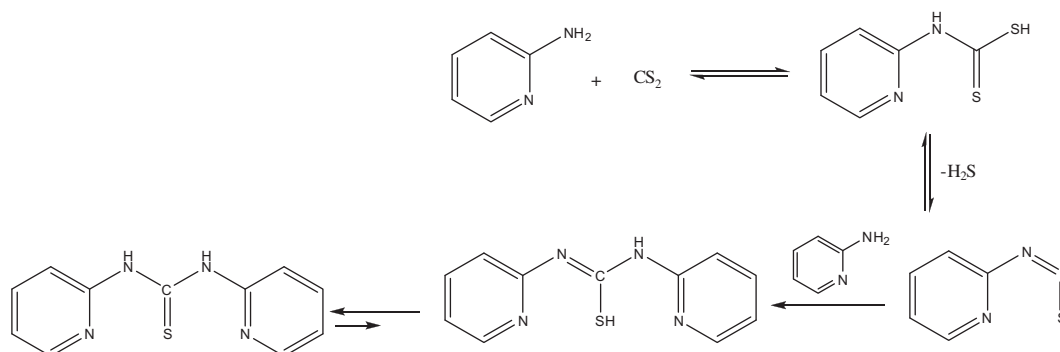


Fig. 2. Synthesis of H_2BPT ligand.

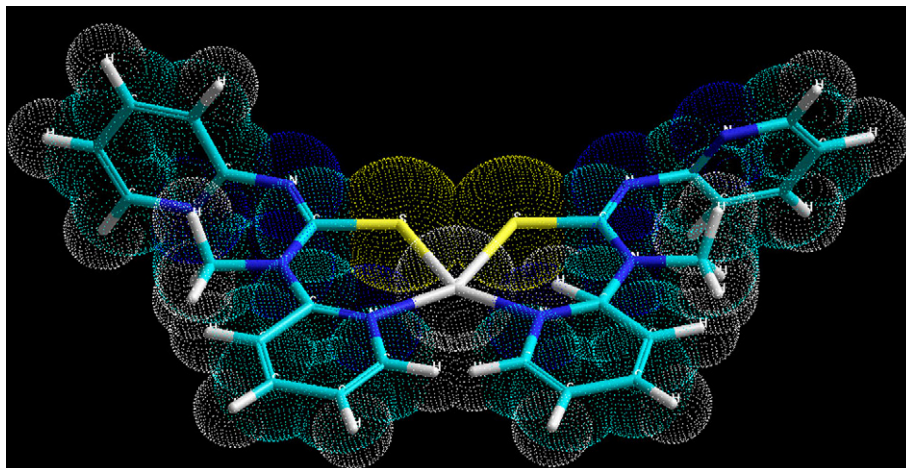


Fig. 3. Structure of [Pt(HBPT)₂].

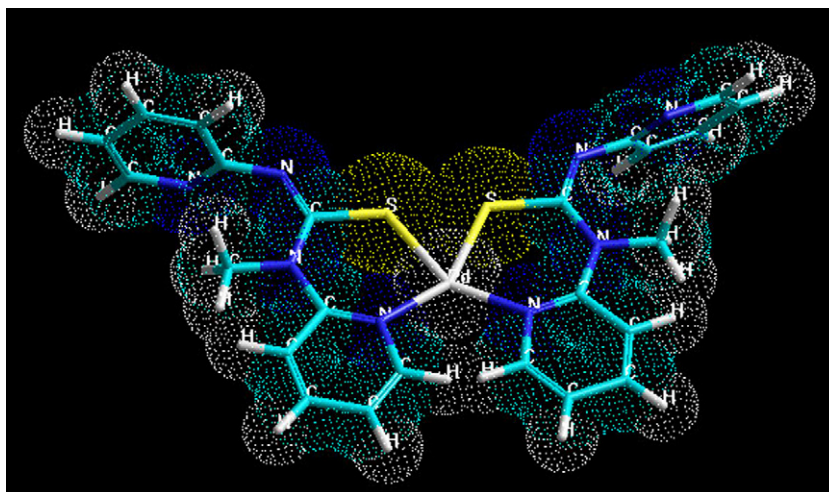


Fig. 4. Structure of [Pd(HBPT)₂].

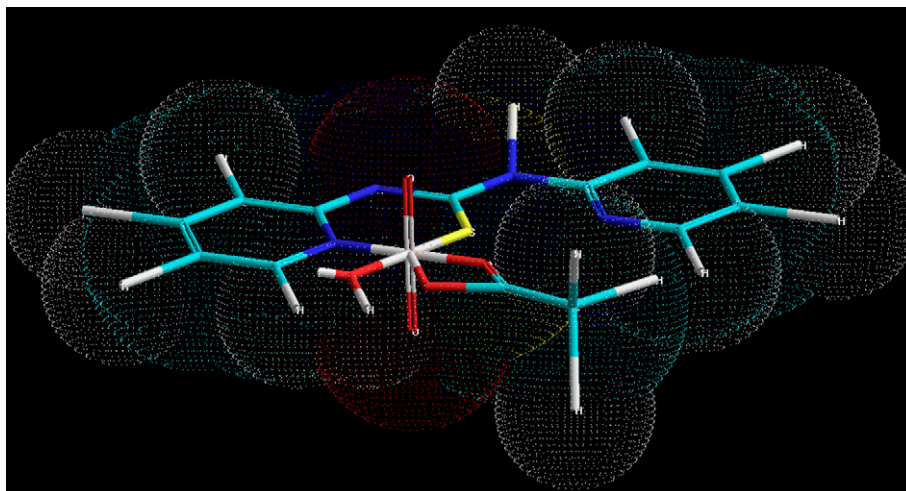


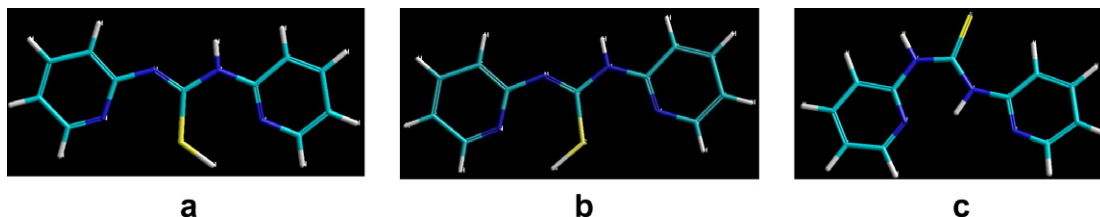
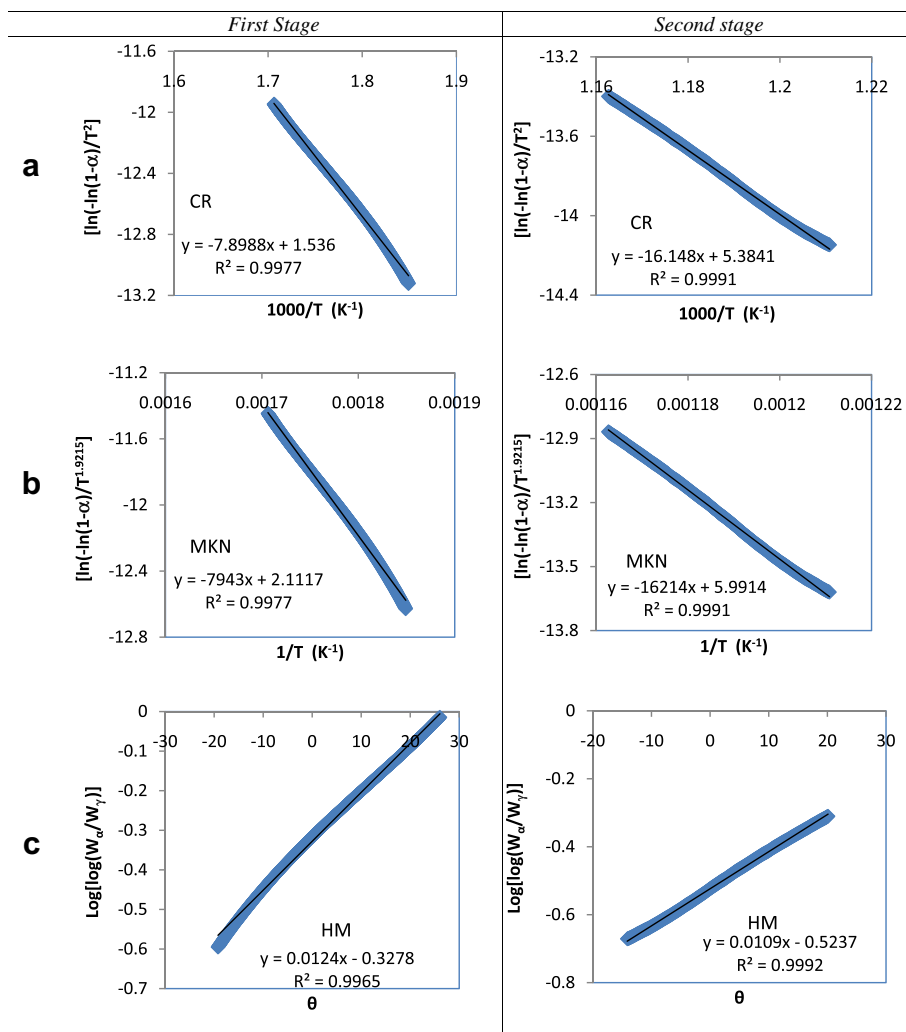
Fig. 5. Structure of [UO₂(HBPT)(OAc)(H₂O)].

diffusion technique [19]. The test was done against the Gram-negative *Escherichia coli* (*E. coli*) and *Pseudomonas aeruginosa* (*P. aeruginosa*) and the Gram-positive *Staphylococcus aureus*

(*S. aureus*) and *Bacillus thuringiensis* (*B. thuringiensis*). The tested free (H₂BPT) ligand or its complexes were dissolved in DMSO at concentration 1 mg/mL. The Luria-Bertani Agar (LBA) medium

Table 1Analytical and physical data and main IR spectral bands of H₂BPT ligand and its metal complexes.

Compound			%Calc. (Found)			$\nu(\text{C}=\text{N})^{\text{PV}}$	$\nu(\text{C}=\text{S})$	$\nu(\text{S}-\text{C}=\text{N})$	$\nu(\text{C}-\text{S})$
Empirical formula	(F. Wt)	Color	C	H	N				
(H ₂ BPT), C ₁₁ H ₁₀ N ₄ S	(230.3)	Off-white	57.37 (57.60)	4.38 (4.30)	24.33 (24.50)	1603	787	–	–
[Pt(HBPT) ₂], C ₂₂ H ₁₈ N ₈ PtS ₂	(653.6)	Yellow	40.40 (40.10)	2.77 (2.69)	17.10 (16.85)	1610, 1630	–	1553	1150
[Pd(HBPT) ₂], C ₂₂ H ₁₈ N ₈ PdS ₂	(564.98)	Orange	46.77 (45.67)	3.21 (3.25)	19.83 (19.77)	1608, 1642	–	1549	1151
[UO ₂ (HBPT)(OAc)(H ₂ O)], C ₁₃ H ₁₄ N ₄ O ₅ SU	(576.4)	Pale-yellow	27.10 (27.50)	2.45 (2.50)	9.72 (10.20)	1616, 1652	–	1555	1150

**Fig. 6.** Possible conformers (A, B and C) of the free ligand H₂BPT.**Fig. 7.** Coats–Redfern (a), MKN (b), and Horowitz–Metzger (c) plots for [Pd(HBPT)₂].

was used. An aliquot of the solution of the tested complexes equivalent to 100 μg was placed separately in each cup. The LBA plates were incubated for 24 h at 37 $^{\circ}\text{C}$ and the resulting inhibition zones

were measured. Ampicillin 1 mg/mL was used as a positive control while DMSO, which exhibited no antibacterial activity, was used as a negative control.

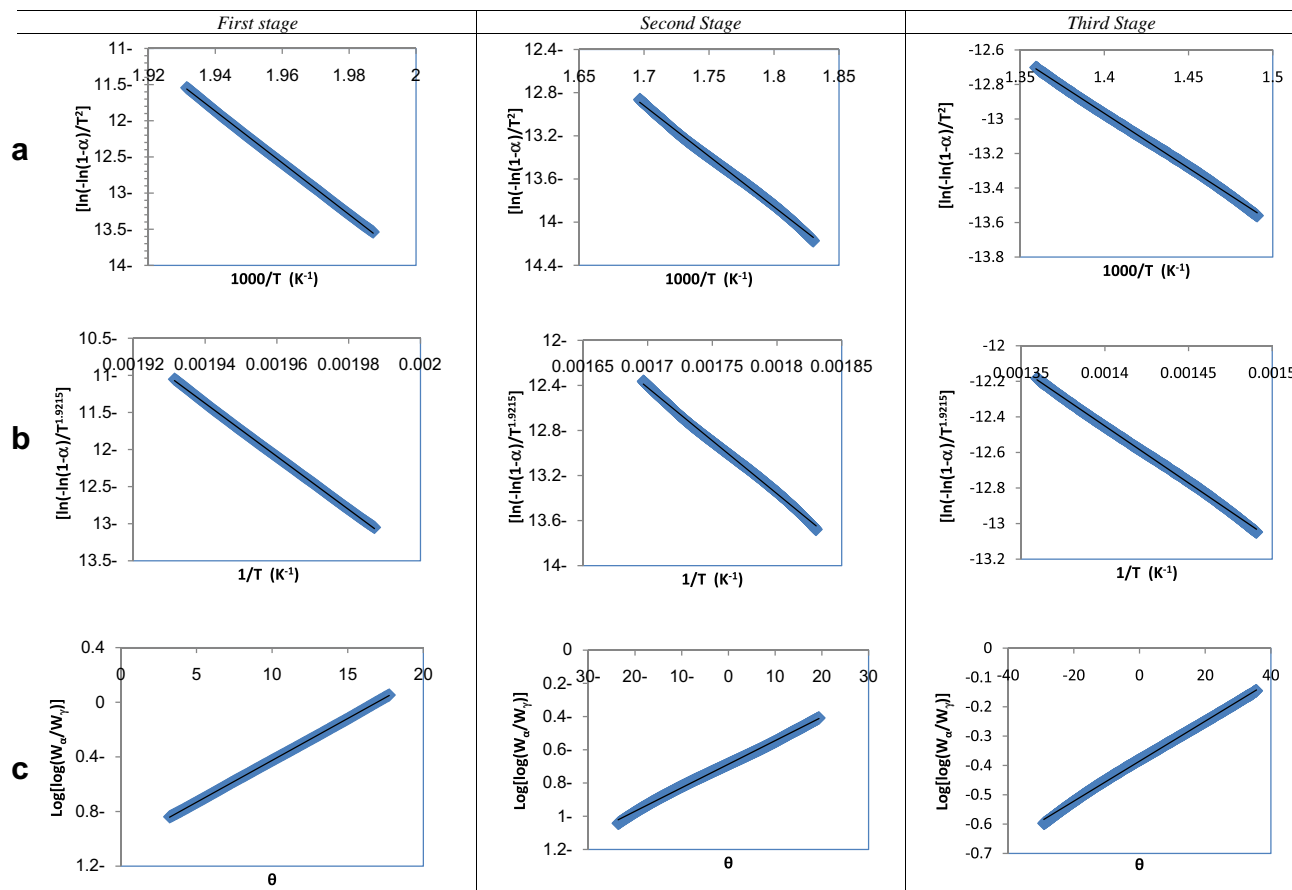


Fig. 8. Coats–Redfern (a), MKN (b), and Horowitz–Metzger (c) plots for [Pt(HBPT)₂].

4. Results and discussion

4.1. IR and NMR spectra of H₂BPT and its metal complexes

Important IR bands for the ligand and complexes with their tentative assignments are presented in Table 1.

Conformational performance of H₂BPT ligand was examined by the rotation and orientation in the space of the flexible *thiourea* and *pyridyl* groups. For such compound the MM calculations led to three minimum energy conformations (Fig. 6) within energy differences of less than 4 Kcal/mol.

The arrangement around the N1–S1 and N2–S1 bonds mainly determine the geometry of the N-substituent groups. So it is clear from the calculation that the conformer A is more stable than B and C with energy content of 19.075, 19.093 and 22.78 Kcal/mol, respectively. Experimentally, ¹H NMR spectra of the ligand confirm the presence of the H₂BPT ligand as conformer A with a signal at 14.21 ppm assigned to SH proton.

H₂BPT behaves as mononegative bidentate ligand coordinating via the nitrogen of the pyridyl group and the CS group in the thiol form. This behavior which is found in all studied complexes is revealed by (i) the ν(C=N)^{py} vibration is observed at 1603 cm⁻¹ for H₂BPT and at 1610, 1630 cm⁻¹ for complex **2**, 1608, 1642 cm⁻¹ for complex **3** and at 1616, 1652 cm⁻¹ for complex **4**. All complexes exhibit two ν(C=N)^{py} peaks, indicating that only one pyridine ring participating in coordination. (ii) The disappearance of ν(C=S) peak with the appearance of new bands due to ν(S–C=N) and ν(C–S).

In complex **4**, a peak is observed at 921.9 cm⁻¹ assigned to the asymmetric stretching frequency (ν₃) of the dioxouranium ion

[20]. The force constant (*F*) for the bonding sites of ν(U=O) is calculated by the method of McGlynn et al. [21].

$$(\nu_3)^2 = (1307)^2(F_{U-O})/14.1$$

The F_{U–O} value is 7.01 m dynes Å⁻¹, the U–O bond distance is calculated with the help of the equation [22] shown below.

$$R_{U-O} = 1.08^{-1/3} + 1.17$$

The U–O bond distance (1.74 Å) falls in the usual region as reported earlier [23,24].

Acetate chelates show two bands at 1541 and 1456 cm⁻¹ assignable to ν_{asym}(COO) and ν_{sym}(COO), respectively. This difference exhibit Δ value [ν_{asym}(COO) – ν_{sym}(COO)] equal to 85 cm⁻¹ that is significantly smaller than the ionic value indicating bidentate chelating acetate group [25,26]. NMR spectrum of this complex shows new signal at δ = 2.86 ppm assigned to the methyl protons indicating the presence of acetate group in the coordination sphere of uranium.

4.2. Electronic spectra of complexes

The electronic spectra of complexes **2** and **3** are indicative of square-planar geometry. In the visible region of the square-planar complexes of Pt(II) and Pd(II), three spin-allowed singlet-singlet d-d transitions are predicted. The ground state is ¹A_{1g}, ¹B_{1g} and ¹E_g in order of increasing energy. Strong charge transfer transition interferes and prevents the observation of all expected bands. The very intense band observed at 22,000–23,000 cm⁻¹ in the electronic spectra of complexes **2** and **3** is assignable to a combination

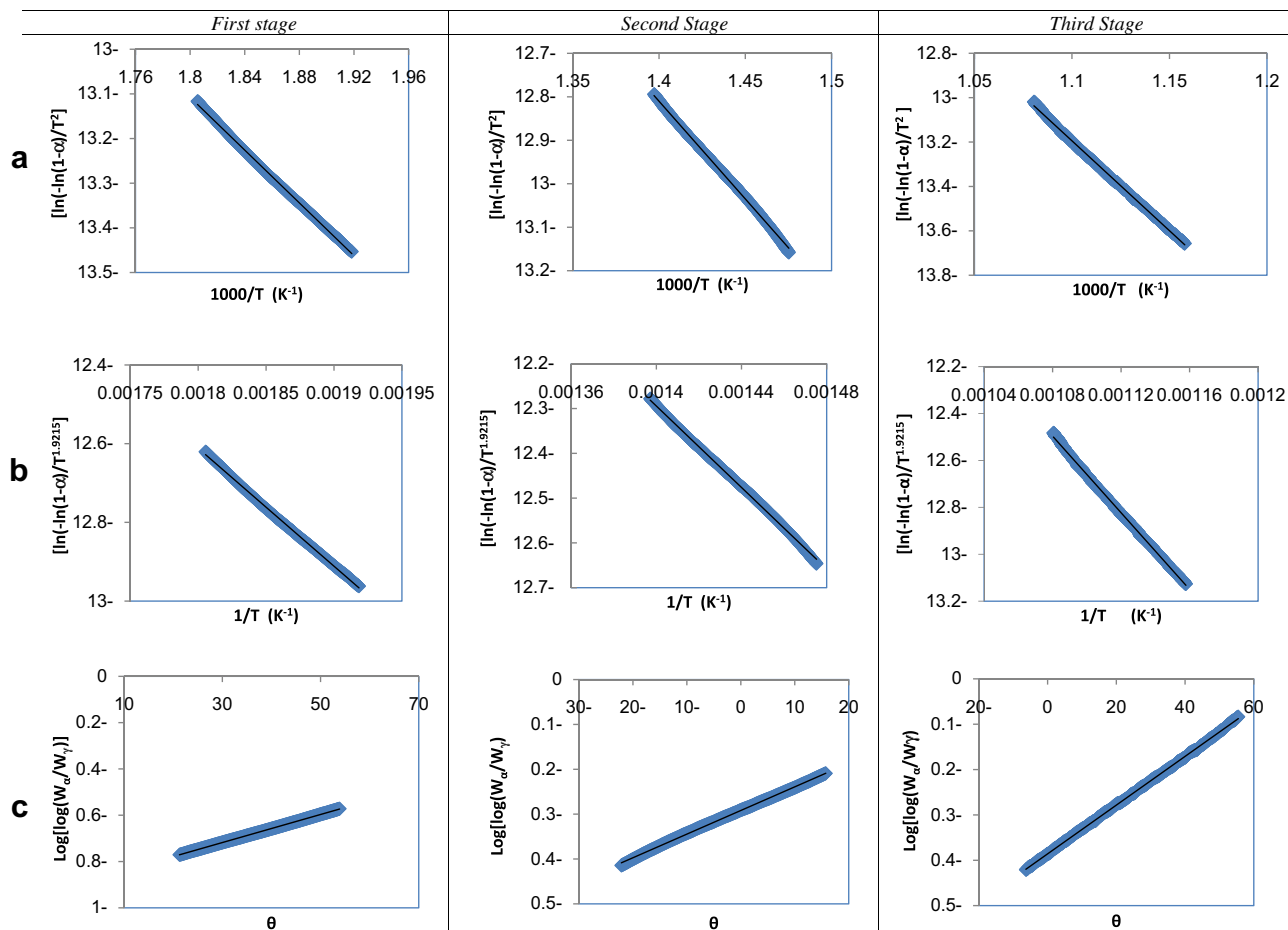


Fig. 9. Coats–Redfern (a), MKN (b), and Horowitz–Metzger (c) plots for $[\text{UO}_2(\text{HBPT})(\text{OAc})(\text{H}_2\text{O})]$.

of sulfur $\rightarrow M(\text{II})$, nitrogen(pyridyl) $\rightarrow M(\text{II})$ charge transfer ($L(\text{II}) \rightarrow M(\text{CT})$) and $M(\text{II})$ $d-d$ bands. The strong bands at $25,000\text{--}27,000\text{ cm}^{-1}$ are assignable to a combination of metal-ligand charge transfer ($M \rightarrow L\text{CT}$) and $d-d$ bands. The band at $32,000\text{--}33,000\text{ cm}^{-1}$ is assignable to the $n \rightarrow \pi^*$ transition of the pyridine ring and the thiourea moiety ($L \rightarrow M\text{CT}$).

The electronic spectra of complex **4** exhibit several bands in the range of $50,000\text{--}14,000\text{ cm}^{-1}$. The bands in the region $50,000\text{--}32,000\text{ cm}^{-1}$ coincide with the bands observed in the free ligand. Some of these bands are slightly shifted towards lower energy region compared to the free ligand transitions because of the coordination with the $\text{U}(\text{VI})$ ion. Since these are essentially the intraligand transitions they are allowed and occur with high intensity. Two relatively less intense bands occur at $22,000\text{--}27,000\text{ cm}^{-1}$. These can be assigned to uranyl oxygen to uranium and pyridyl nitrogen to uranium charge transfer transitions, respectively.

4.3. Molecular modeling studies

An attempt to gain a better insight on the molecular structures of the (**2–4**) complexes, conformational analysis of the target compounds have been performed by MM + force field as implemented in HyperChem 7.5. The results show that the lowest energy conformer as calculated by PM3 semiempirical method of both (**2** and **3**) complexes have approximate atomic coordinates. The calculations performed indicate that the pyridyl groups, showing highly free rotations, were spatially arranged itself approximately coplanar and perpendicular to the plane of core complex. This unique arrangement may be stabilized by nonbonded interaction;

CH/II interaction of methyl group with pyridine ring (2.6 \AA). This nonbonded interaction may be the reason for the coplanarity of the dipyridyl groups and this factor may be strong enough to compensate the steric repulsion. On the other hand, the calculation on complex **4**, dipyridyl groups were arranged itself coplanar. This coplanar orientation of is caused by the presence of strong $\text{S}\text{--}\text{N}$ interaction (1.42 \AA), which prevents rotation of pyridyl moiety in the plane formed by the complex core.

4.4. Thermal behavior and the decomposition kinetics

TG/DTG curves of the complexes showed that complex **3** decomposes in two steps, while complexes **2** and **4** are decomposes in three steps.

In studying the decomposition kinetics, three methods namely, Coats–Redfern (CR), Horowitz–Metzger (HM) and MKN were used. In these methods (CR, HM and MKN) the left-hand side of equations 6, 9 and 11 is plotted against $1000/T$, θ and $1/T$, respectively (Figs. 7–9). From the results obtained, the following remarks can be pointed out: (i) the kinetic parameters (E , A , ΔH , ΔS and ΔG) of all studied complexes have been determined (Table 2) using CR, HM and MKN methods. The values obtained from the three methods are quite comparable. (ii) All complexes decomposition stages show a best fit for ($n = 1$) indicating a first-order decomposition in all cases. Other n values (e.g. 0, 0.33 and 0.66) did not lead to better correlations. (iii) The value of ΔG increases significantly for the subsequently decomposition stages of a given complex. This is due to increasing the value of $T\Delta S$ significantly from one stage to another which overrides the value of ΔH . Increasing the value of ΔG of a

Table 2
Kinetic parameters of H₂BPT ligand and its metal complexes.

Complex	Stage	T (K)	A (S ⁻¹)	E (KJmol ⁻¹)	ΔH (KJmol ⁻¹)	ΔS (KJmol ⁻¹)	ΔG (KJmol ⁻¹)
<i>Coats–Redfern method</i>							
[Pd(HBPT) ₂]	1st	560	6.2 × 10 ³	65.7	61.0	-0.186	165.1
	2nd	840	6.0 × 10 ⁵	134.2	127.2	-0.151	254.3
[Pt(HBPT) ₂]	1st	500	5.8 × 10 ²⁸	297.3	293.2	0.293	146.6
	2nd	570	3.3 × 10 ⁴	78.0	73.2	-0.172	171.4
	3rd	700	18.39	52.8	47.0	-0.236	212.3
[UO ₂ (HBPT)(OAc)(H ₂ O)]	1st	500	0.20	24.5	20.4	-0.271	155.7
	2nd	700	1.13	37.4	31.5	-0.259	213.1
	3rd	870	19.0	67.3	60.1	-0.238	266.9
<i>Horowitz–Metzger method</i>							
[Pd(HBPT) ₂]	1st	560	7.4 × 10 ³	65.9	61.3	-0.184	164.6
	2nd	840	6.9 × 10 ⁵	134.7	127.7	-0.150	253.7
[Pt(HBPT) ₂]	1st	500	6.0 × 10 ²⁸	297.4	293.2	0.293	146.5
	2nd	570	3.8 × 10 ⁴	78.2	73.2	-0.171	170.9
	3rd	700	22.66	53.2	47.4	-0.234	211.5
[UO ₂ (HBPT)(OAc)(H ₂ O)]	1st	500	0.29	24.9	20.7	-0.268	155.0
	2nd	700	1.43	37.8	31.9	-0.257	212.1
	3rd	870	23.42	67.9	60.6	-0.236	265.9
<i>MKN Method</i>							
[Pd(HBPT) ₂]	1st	560	2.4 × 10 ⁴	72.0	67.4	-0.174	165.1
	2nd	840	9.9 × 10 ⁵	135.1	128.1	-0.147	251.7
[Pt(HBPT) ₂]	1st	500	7.6 × 10 ²⁸	292.0	287.9	0.295	140.1
	2nd	570	5.2 × 10 ⁵	87.1	82.4	-0.149	167.4
	3rd	700	37.3	56.3	50.4	-0.230	211.6
[UO ₂ (HBPT)(OAc)(H ₂ O)]	1st	500	2.35	28.7	24.6	-0.250	149.8
	2nd	700	6.20	46.9	41.1	-0.245	212.7
	3rd	870	43.90	72.5	65.2	-0.231	265.9

given complex on going from one decomposition step subsequently to another reflects that the rate of removal of the subsequent ligand will be lower than that the precedent ligand [27,28]. This may be attributed to the structure rigidity of the remaining complex after the explosion of one and more ligands, as compared with the precedent complex, which require more energy, $T\Delta S$, for its rearrangement before undergoing any compositional change. (iv) The negative value of activation entropies ΔS indicates a more ordered activated complex than the reactants and/or the reactions are slow [29]. (v) The positive value of ΔH means that the decomposition processes are endothermic. (vi) The energy of activation values E for the second step of decomposition of complex **3** and complex **4** are found to be higher than that of the first stage indicating that the rate of decomposition for this stage is lower than that for the first stage. In case of complex **2**, the energy of activation for the second stage is lower than the first step. This confirms that the rate of decomposition is higher in the second step [30].

It is generally observed that stepwise stability constants decrease with an increase in the number of ligands attached to the metal ion [31,32]. During the decomposition reaction a reverse effect may occur. Hence the rate of removal of the remaining ligands will be smaller after the explosion of one or two ligands.

4.5. Ionic radius/thermal stability

From the data obtained in this work, it was possible to show the relation between thermal stability of complexes and their metal ion radii. The higher the ionic radius of the metal ion in the complex, the lower was the initial decomposition temperature of the complex as measured by TG, in the following order of thermal stability complex **2** (ionic radius of 74 pm and initial decomposition temperature of 200 °C) > complex **3** (ionic radius of 78 pm and initial decomposition temperature of 100 °C) > complex **4** (io-

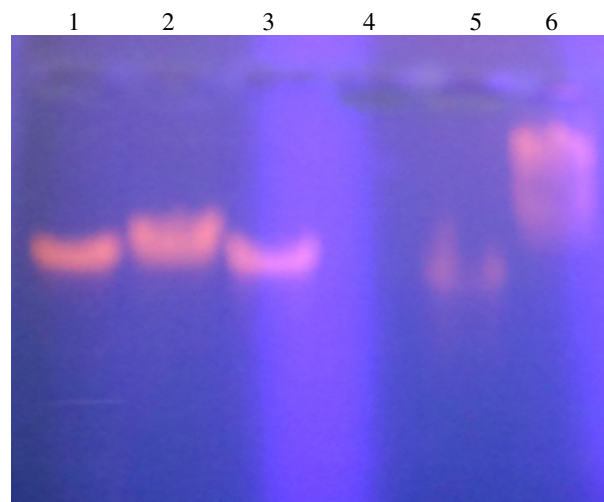


Fig. 10. Effect of 100 μM of H₂BPT free ligand and its metal complexes on the DNA *in vitro*.

nic radius of 87 pm and initial decomposition temperature of 70 °C).

4.6. Biochemical effect of H₂BPT ligand and its metal complexes on the DNA *in vitro*

The degradation effect of 100 μM of the free (H₂BPT) ligand **1**, and its (**2–4**) complexes on the DNA *in vitro* illustrated in Fig. 10. Both the -ve control (only DNA) and +ve control (DNA in DMSO) does not exhibit any degradation through the incubation period as illustrated in Fig. 10 lanes 1 and 2, respectively. The Pt(II) complex **2** has a powerful and complete degradation effect on

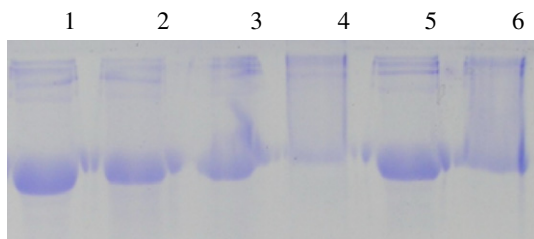


Fig. 11. Effect of 100 μM of H_2BPT free ligand and its metal complexes on the BSA protein *in vitro*.

Table 3

The antimicrobial effect of H_2BPT legand and its metal complexes on some microorganisms. The results are expressed as zone inhibition in millimeter diameter.

Compound	<i>E. coli</i>	<i>P. aeruginosa</i>	<i>S. aureus</i>	<i>B. thuringiensis</i>
Ampicillin	16	13	12	14
H_2BPT , 1	7	6	6	–ve
$[\text{Pt}(\text{HBPT})_2]$, 2	9	12	12	11
$[\text{Pd}(\text{HBPT})_2]$, 3	–ve	–ve	–ve	–ve
$[\text{UO}_2(\text{HBPT})(\text{OAc})(\text{H}_2\text{O})]$, 4	–ve	–ve	–ve	–ve

the DNA as illustrated in Fig. 10 lane 4. Therefore complex **2** can be used as a promising anti-tumor agent *in vivo* to inhibit the DNA replication in the cancer cells and not allow the tumor for further growth. The Pd(II) complex **3** has a strong degradation effect on the DNA as represented in lane 5 compared with the free ligand lane 3. The $\text{UO}_2(\text{II})$ complex **4** has a partial degradation effect on the DNA as observed in lane 6.

Further biochemical studies to illustrate the exact role of the promising degradation effect by complexes **2** and **3** on tumor cells were carried out. Therefore, we decided to study the effect of these compounds on the protein as another important macromolecule. The effect of the free (H_2BPT) ligand **1**, and its (**2–4**) complexes on the BSA was carried out and the results were shown in Fig. 11.

The BSA protein is not affected by DMSO as a solvent, lanes 1 and 2 respectively. Complex **3** has no apparent degradation effect on the BSA protein (Fig. 11 lane 5). Complex **4** exhibited a moderate degradation effect on BSA while the free (H_2BPT) ligand **1**, has little cleavage effect on the BSA (Fig. 11 lanes 6 and 3 respectively). Strong degradation effect was observed with complex **2** as represented in Fig. 11 lane 4.

The free ligand exhibited antimicrobial activity against bacterial strains *Escherichia coli* (*E. coli*), *Staphylococcus aureus* (*S. aureus*) and *Pseudomonas aeruginosa* (*P. aeruginosa*) as listed in Table 3. Complex **2** give a strong antimicrobial activity against all studied bacterial strains compared with ampicillin as antimicrobial drug. Complexes **3** and **4** do not show any antimicrobial activity against all tested bacterial strains.

Cisplatin has been used in the treatment of many cancers. Upon entering the cell, cisplatin becomes positively charged, and so is able to interact with nucleophilic molecules including DNA, RNA and proteins. In the present study, platinum complex (complex **2**) was demonstrated to degrade the *in vitro* DNA and protein. Complex **2** may interact with DNA as the same way of cisplatin, forming inter- and intra-strand adducts, hindering DNA replication, leading to cell cycle arrest and apoptosis.

5. Conclusion

Novel complexes of Pt^{2+} , Pd^{2+} and U^{6+} with *N,N'*-bis(2-pyridyl)thiourea (H_2BPT) **1** were synthesized. Geometry optimization and conformational analysis have been performed and a perfect agreement with spectral studies and analytical measurements allow for suggesting the exact structure of all studied complexes. The stability of complexes was explained and the kinetic parameters (E , A , ΔH , ΔS and ΔG) of all thermal decomposition stages have been evaluated using Coats–Redfern, Horowitz–Metzger and MKN methods. The results shows that the kinetic parameters (Table 2) evaluated by all three methods are in a very good agreement. The biological studies showed that Pt(II) complex has a powerful and complete degradation effect on DNA “which maybe a sign for anti-tumor activity”. Moreover, the antibacterial screening demonstrated that, Pt(II) complex has the maximum and broad range activities against Gram-positive and Gram-negative bacterial strains.

Acknowledgements

The financial support by the Deanship of Scientific Research (Project Number 10080) King Faisal University, Saudi Arabia, is gratefully acknowledged. Thanks are due to Dr. Magdy M. Youssef, Chemistry department, Faculty of Science, for the help with biological studies.

References

- [1] A. Saxena, R.D. Pike, *J. Chem. Crystallogr.* 37 (2007) 755.
- [2] X.X. Zhou, Y.M. Liang, F.J. Nan, Y.X. Ma, *Polyhedron* 11 (1992) 447.
- [3] Y. Omote, *Bull. Chem. Soc. Jpn.* 46 (1973) 2896.
- [4] B. Grag, *Inorg. Chem. Acta* 170 (1990) 177.
- [5] D.X. West, A.K. Hermetet, L.J. Ackerman, J. Valdes-Martinez, S. Hernandez-Ortega, *Acta Cryst. C55* (1999) 811.
- [6] D.X. West, J.K. Swearingen, A.K. Hermetet, L.J. Ackerman, C. Presto, *J. Mol. Struct.* 522 (2000) 27.
- [7] D.X. West, J.K. Swearingen, A.K. Hermetet, L.J. Ackerman, *J. Mol. Struct.* 562 (2001) 95.
- [8] Y. Fan, H. Lu, H. Hou, Z. Zhou, Q. Zhao, L. Zhang, F. Cheng, *J. Coord. Chem.* 50 (2000) 65.
- [9] J. Sestak, V. Satava, W.W. Wendalndt, *Thermochim. Acta* 7 (1973) 333.
- [10] A.W. Coats, J.P. Redfern, *Nature* 201 (1964) 68.
- [11] H.H. Horowitz, G. Metzger, *Anal. Chem.* 35 (1963) 1464.
- [12] P.M. Madhusudanan, K. Krishnan, K.N. Ninan, *Thermochim. Chem. Acta* 97 (1986) 189.
- [13] J.H.F. Flynn, L.A. Wall, *J. Res. Nat. Bur. Stand.* 70A (1996) 487.
- [14] A.M. Summan, *Thermochim. Chem. Acta* 285 (1996) 119.
- [15] N.L. Allinger, *J. Am. Chem. Soc.* 99 (1977) 8127.
- [16] HyperChem Professional 7.5, Hypercube, Inc., Gainesville, FL 32601, USA, 2002. <<http://www.hyper.com>>.
- [17] J. Sambrook, E.F. Fritsch, T. Maniatis, *Molecular Cloning: A Laboratory Manual*, Cold Spring Harbor Laboratory Press, Cold Spring Harbor, NY, 1989.
- [18] U.K. laemmli, *Nature* 227 (1970) 689.
- [19] A.W. Bauer, W.M. Kirby, J.C. Sherris, M. Turck, *Am. J. Clin. Pathol.* 45 (1966) 493.
- [20] F. Quilés, *Vib. Spectro.* 18 (1998) 61.
- [21] S.P. McGlynn, J.K. Smith, W.C. Neely, *J. Chem. Phys.* 35 (1961) 105.
- [22] L.H. Jones, *Spectrochim. Acta* 11 (1959) 409.
- [23] U. El-Ayaan, M.M. Youssef, S. Al-Shihry, *J. Mol. Struct.* 936 (2009) 213.
- [24] G.A. El-Reash, U. El-Ayaan, I.M. Gabr, E. El-Rachawy, *J. Mol. Struct.* 969 (2010) 33.
- [25] K. Nakamoto, *Infrared and Raman Spectra of Inorganic and Coordination Compounds Part B*, Wiley, New York, 2009. p. 64.
- [26] N.W. Alcock, J. Culver, S.M. Roe, *J. Chem. Soc. Dalton Trans.* (1992) 1477.
- [27] P.M. Maravalli, T.R. Goudar, *Thermochim. Acta* 325 (1999) 35.
- [28] K.K.M. Yusuff, R. Sreekala, *Thermochim. Acta* 159 (1990) 357.
- [29] A.A. Frost, R.G. Pearson, *Kinetics and Mechanism*, Wiley, New York, 1961.
- [30] A.H.M. Siddalingaiah, Sunil G. Naik, *J. Mol. Struct.* 582 (2002) 129.
- [31] V. Indira, G. Parameswaran, *J. Therm. Anal.* 29 (1984) 3.
- [32] R. Sreekala, K.K.M. Yusuf, *React. Kinet. Lett.* 48 (2) (1992) 575.